

## **Reconstruction of spinel $\text{Co}_3\text{O}_4$ by inert $\text{Zn}^{2+}$ towards enhanced oxygen catalytic activity**

Yifan Wang,<sup>a, b</sup> Ze-Pan Wang,<sup>b</sup> Huixiang Wu,<sup>b</sup> Liping Hou,<sup>\*, a</sup> Zhao-Qing Liu<sup>\*, b</sup>

<sup>a</sup>School of Life Science, Guangzhou University, Guangzhou 510006, P. R. China

<sup>b</sup>School of Chemistry and Chemical Engineering/Institute of Clean Energy and Materials/Guangzhou Key Laboratory for Clean Energy and Materials, Guangzhou University, Guangzhou 510006, P. R. China.

E-mail: [Houliping7710@163.com](mailto:Houliping7710@163.com) (L. P. Hou); [lzqgz@gzhu.edu.cn](mailto:lzqgz@gzhu.edu.cn) (Z. Q. Liu)

## Content

### Experimental Section

|   |   |
|---|---|
| 1.1 Synthesis of catalysts.....               | 3 |
| 1.2 Physicochemical<br>Characterizations..... | 3 |
| 1.3 Electrochemical<br>measurements.....      | 4 |

### Supplementary Figures

|  |    |
|--|----|
| Figure S1. SEM of samples.....   | 6  |
| Figure S2. XRD pattern of<br>NHCS.....   | 7  |
| Figure S3. XRD and Raman spectra of<br>samples.....                                      | 7  |
| Figure S4. The Brunauer-Emmett-Teller and aperture analysis of<br>samples.....           | 8  |
| Figure S5. XPS deconvolution analyze of Co.....  | 9  |
| Figure S6. XPS spectrum and the ratio of $\text{Co}^{2+}/\text{Co}^{3+}$ in samples..... | 10 |
| Figure S7. ORR catalytic performance and error analysis .....                            | 11 |
| Figure S8. CV curves of samples at different scan rates.....                             | 11 |
| Figure S9. The stability of ORR test of samples.....                                     | 12 |
| Figure S10. OER catalytic performance and error analysis.....                            | 13 |
| Figure S11. OER CV curves.....   | 13 |
| Figure S12. The stability of OER test of .....   | 14 |
| Figure S13. The amount of dissolved Zn in the sample after 1500 cycles.....              | 14 |
| Figure S14. The scheme of rechargeable Zn–air battery.....                               | 15 |
| Figure S15. Parameter of battery of<br>catalysts.....                                    | 15 |

## **Supplementary Tables**

Table S1. Comparison for ORR activity of catalysts.....16

Table S2. Comparison for OER activity of catalysts.....17

**Reference**.....18

## Experimental Section

### 1.1 Synthesis of NHCS

The NHCS precursor was synthesized by the polymerization of resorcinol/formaldehyde (RF) in a mixture of alcohol and aqueous ammonia. First, 0.4 g of resorcinol was dissolved in stirring solution composed of 70 mL of ethanol, 10 mL of deionized water, and 3 mL of ammonia and stirred for 5 min at room temperature. Subsequently, formaldehyde (0.56 mL) and 2.8 mL tetraethyl orthosilicate were added continuously to form a formaldehyde/resorcinol layered resin together with SiO<sub>2</sub> (RF@SiO<sub>2</sub>). To increase the number of mesopores on the surface of RF@SiO<sub>2</sub>, tetraethyl orthosilicates (0.5 mL) was added after stirring for 6 h. RF@SiO<sub>2</sub> reacted for 16 h continuously under alkaline conditions before centrifugation. The collected products were dried at 50 °C for 12 h and then carbonized at 800 °C for 2 h under a nitrogen atmosphere. Finally, after removing the silica template by 6 M NaOH by etching at 70 °C for 6 h, NHCS was successfully synthesized.

### 1.2 Synthesis of Zn<sub>x</sub>Co<sub>3-x</sub>O<sub>4</sub>/NHCS

50 mg of the above-mentioned NHCS, x mmol (Zn (NO<sub>3</sub>)<sub>2</sub>), (3-x) mmol (Co (NO<sub>3</sub>)<sub>2</sub>) and 700 μL NH<sub>3</sub>·H<sub>2</sub>O dissolved in 96 mL ethanol and stirred until a clear solution. Then the mixture kept 80 °C for 20 h. After that, the reaction mixture was transferred to a 100 mL autoclave for hydrothermal reaction at 140 °C for 3 h. The resulting product was collected by centrifugation and washed with ethanol and water, and dried by lyophilization.

### 1.3 Characterizations

The morphology and microstructure of the as-obtained samples were evaluated using field-emission scanning electron microscopy (FE-SEM, JEOL JSM-7001F) and transmission electron microscopy (TEM, JEM2010-HR). X-ray diffraction (XRD, PANalytical, PW3040/60 diffractometer) with monochromatic Cu Kα radiation (λ

=0.15418 nm) was used to analyze the crystal structures of the catalysts. X-ray photoelectron spectroscopy (XPS, ESCALab250) was used to determine the surface chemical states and electronic states of the prepared products. The specific surface areas and pore size distributions of the samples were estimated by Brunauer-Emmett-Teller (BET) analysis.

#### 1.4 Electrochemical measurements

The AMETEK Princeton Applied Research PMC 2000A connected with the three-electrode was used to measure the catalytic activity for ORR and OER. The Hg/HgO electrode was used as the reference electrode, a carbon rod as the counter, and a glassy carbon as the working electrodes. The electrocatalytic activity for the ORR was conducted under O<sub>2</sub> saturation in 0.1 M KOH at a scan rate of 10 mV s<sup>-1</sup> at room temperature (~25 °C) and a rotation rate of 1600 rpm. The OER performance of the catalysts was estimated from LSV in 1 M KOH solution at a scan rate of 10 mV s<sup>-1</sup>. Before recording the ORR and OER polarization plots, cyclic voltammetry at a scan rate of 50 mV s<sup>-1</sup> was performed to activate the catalysts until the catalyst sample reached a steady state. After data collection, IR compensation correction and background correction were performed to evaluate the true OER and ORR catalytic activity.<sup>1</sup> Three parallel experiments were conducted for separately prepared working electrodes to eliminate accidental error. The electrochemical impedance spectroscopy (EIS) was measured at the open circuit potential (OCP) with the AC amplitude of 5 mV during the frequency of 0.01 Hz to 100 kHz.

All potentials in this study are converted to RHE according to the Nernst equation.<sup>2-7</sup>

$$E_{RHE} (V) = E_{Hg/HgO} + 0.098 + 0.059 \times pH$$

The electrochemical surface area (ECSA) of catalysts was obtained by the cyclic voltammetry curves in the non-faraday current region at the scan rates from 2 to 10 mV s<sup>-1</sup>. The relation between current and scan rates is the following equation:

$$C_{dl} = i_c / \nu$$

$i_c$  refers to the non-faraday current;  $C_{dl}$  is the electrochemical double-layer capacitance;  $v$  is the scan rates.

The electron transfer number ( $n$ ) and  $H_2O_2$  yield of catalysts were estimated through ORR by the RRDE method using the following equation:

$$n = 4 \times \frac{I_D}{I_D + I_R/N}$$

$$H_2O_2(\%) = 200 \times \frac{I_R/N}{I_R/N + I_D}$$

where  $n$ ,  $I_d$ ,  $I_R$ , and  $N$  represent the mean electron transfer number of the ORR, disk electrode current, ring electrode current, and collection efficiency of the RRDE (34%), respectively.

The measurements of rechargeable Zn–air batteries were performed on home-built electrochemical cells. All data was collected from the as-fabricated cell using a CHI 760D electrochemical workstation (CH Instruments, Inc., Shanghai, China) at room temperature. Zinc foil was used as the anode, and catalysts loaded on the gas diffusion layer (Nafion-coated carbon fiber paper with a geometric area of  $1 \text{ cm}^2$ , catalyst loading amount of  $6.0 \text{ mg cm}^{-2}$ ) was used as the air cathode. For comparison, the noble metal catalyst consisted of 3 mg Pt/C, 3 mg  $IrO_2$ , and 6.0 M KOH as the electrolyte.

### Supplementary Figures

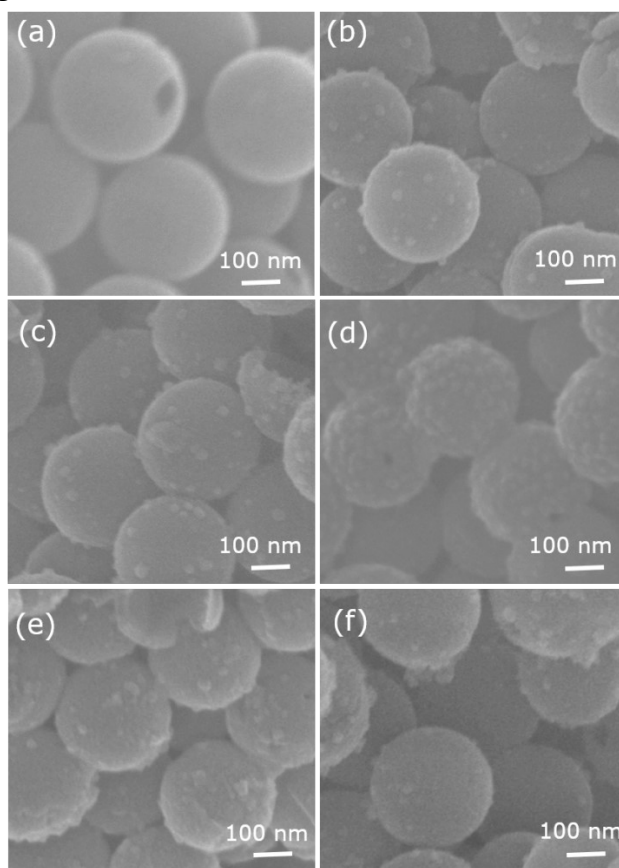


**Figure S1.** SEM images of (a) NHCS, and (b-f) a series of samples.  $Zn_xCo_{3-x}O_4/NHCS$ : b)  $x=0$ , c)  $x=0.3$ , d)  $x=0.6$ , e)  $x=0.8$ , f)  $x=1.0$ .

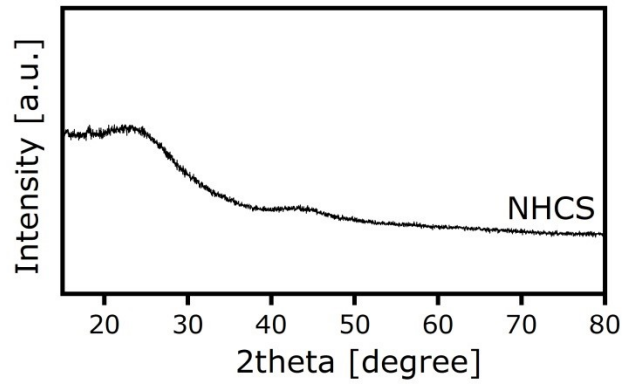


**Figure S2.** XRD pattern of NHCS.

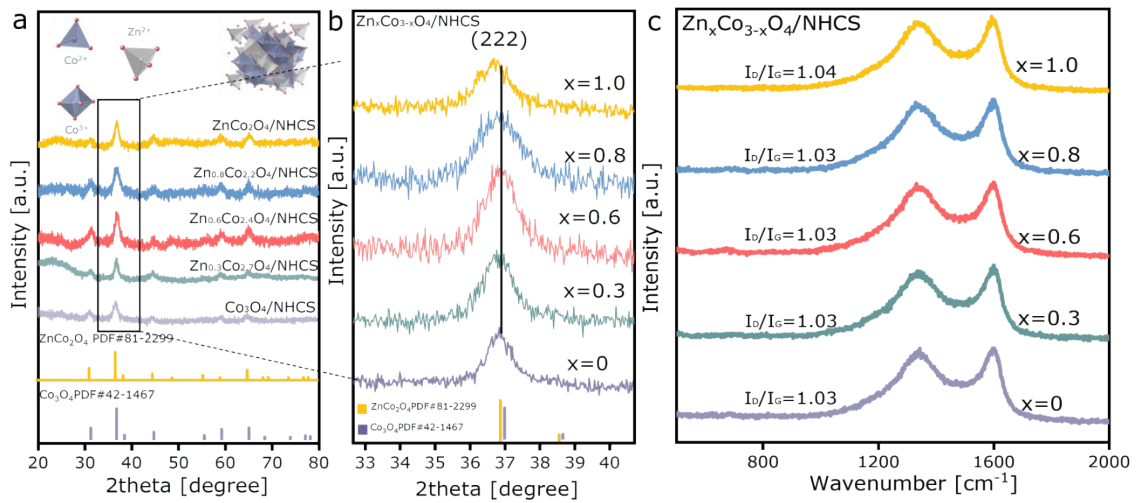


**Figure S3.** (a) XRD pattern of  $Zn_xCo_{3-x}O_4/NHCS$ , (b) the enlarged XRD of  $Zn_xCo_{3-x}O_4/NHCS$ , (c) Raman spectra of  $Zn_xCo_{3-x}O_4/NHCS$ .

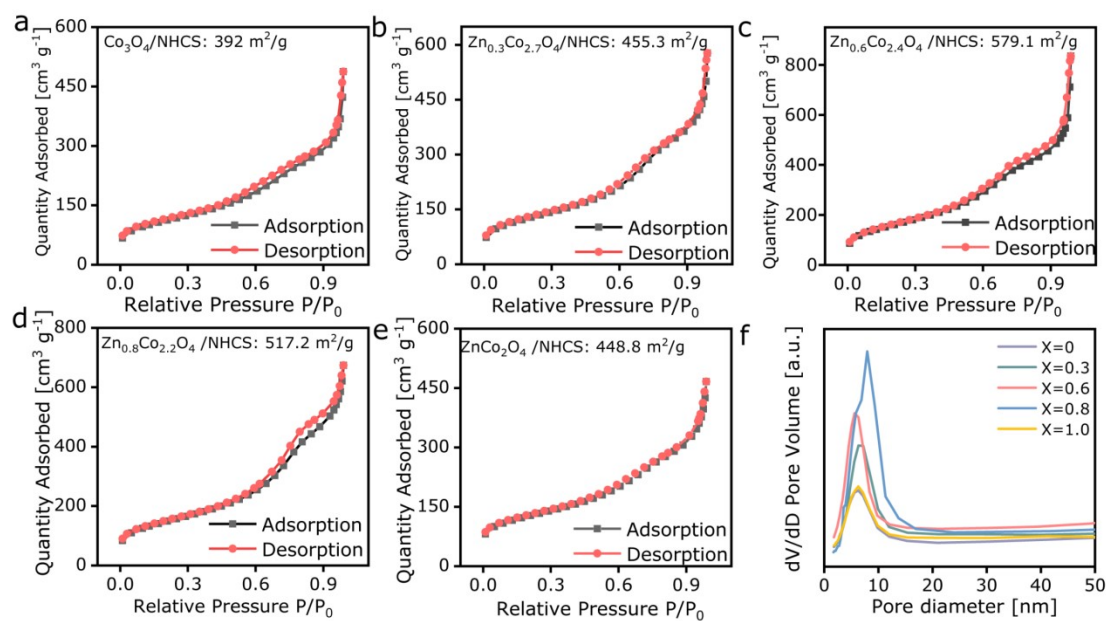


**Figure S4.** (a-e) N<sub>2</sub> adsorption/desorption isotherm of Zn<sub>x</sub>Co<sub>3-x</sub>O<sub>4</sub>/NHCS, and (f) corresponding pore size distribution.

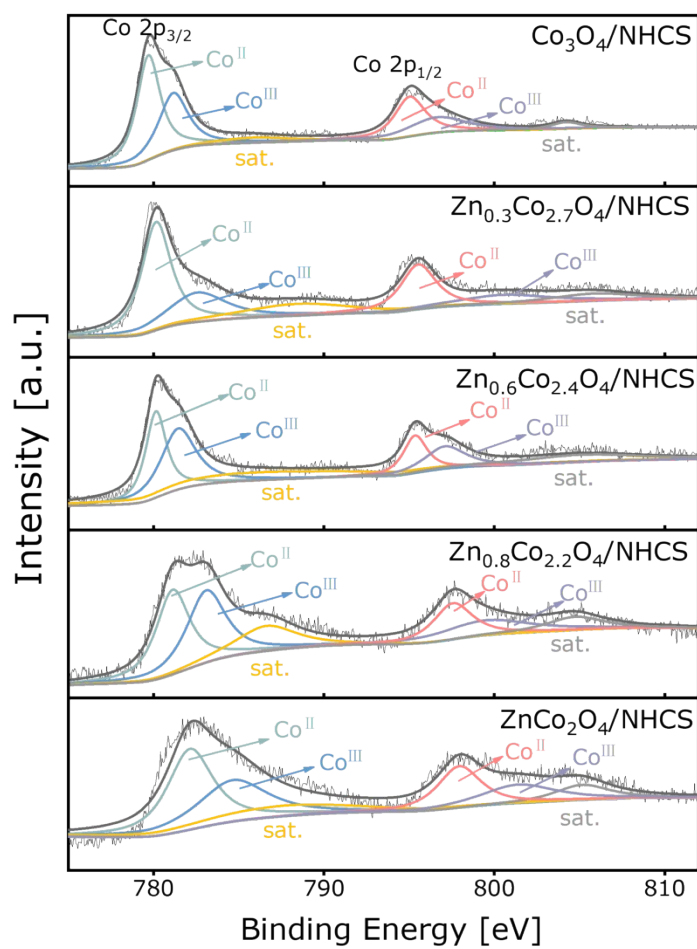


**Figure S5.** High-resolution XPS spectra of Co 2p.

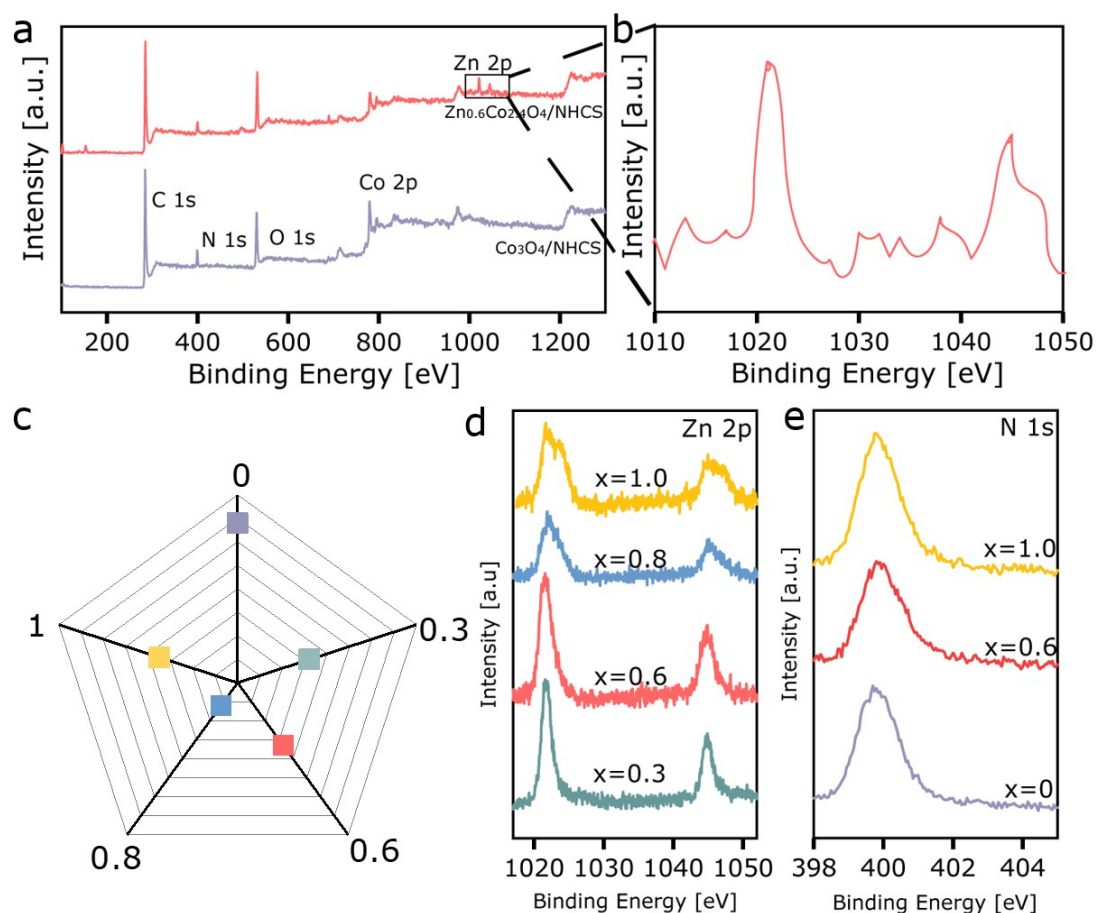


**Figure S6.** (a) Survey XPS spectra of  $\text{Co}_3\text{O}_4/\text{NHCS}$  and  $\text{Zn}_{0.6}\text{Co}_{2.4}\text{O}_4/\text{NHCS}$ , (b) the enlarged survey XPS spectra, (c) the ratio of  $\text{Co}^{2+}/\text{Co}^{3+}$  in samples, (d) Zn 2p XPS spectra, (e) N 1s XPS spectra.

The survey XPS spectra confirmed the presence of Co and O elements in  $\text{Co}_3\text{O}_4/\text{NHCS}$ , Co, O and Zn in  $\text{Zn}_{0.6}\text{Co}_{2.4}\text{O}_4/\text{NHCS}$  (Figure S6b). The Zn 2p XPS spectrum (Figure S6d) showed two peaks with binding energies of approximately 1020 eV (Zn  $2p_{3/2}$ ) and 1043 eV (Zn  $2p_{1/2}$ ), indicating that  $\text{Zn}^{2+}$  exists in a stable oxidation state by losing two electrons from the 4s orbital.<sup>8</sup> The presence of a N 1s peaks at 398.8 eV indicated the formation of N-doped carbon materials (Figure S6e).<sup>9</sup> The introduction of N can assure high conductivity beneficial for rapid electron transfer and provide a large number of N surface sites for the growth and dispersion of high catalytic activity spinel nanoparticles.<sup>10</sup>

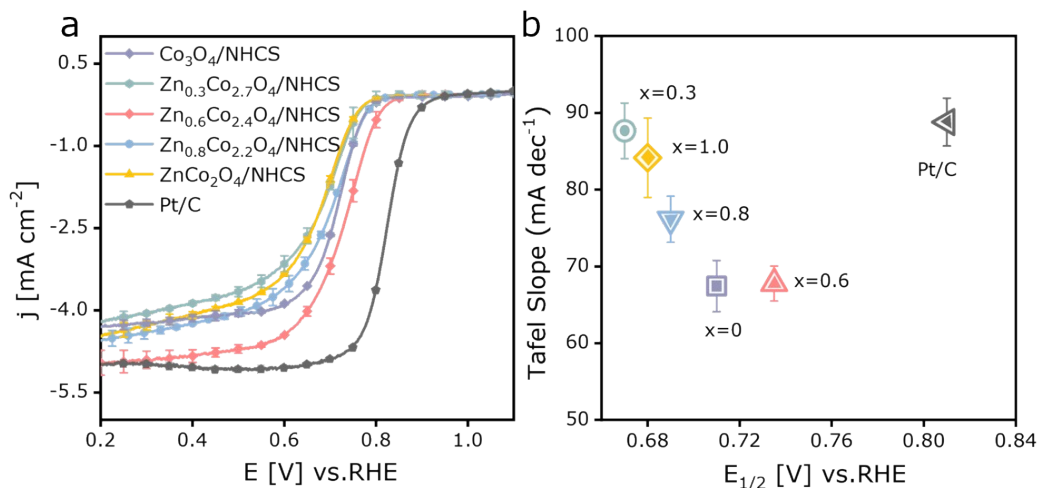


**Figure S7.** (a) ORR polarization curves of  $Zn_xCo_{3-x}O_4/NHCS$  and Pt/C in  $O_2$ -saturated 0.1 M KOH, (b) corresponding Tafel plots. Error bars represent the standard deviation from at least three independent measurements.

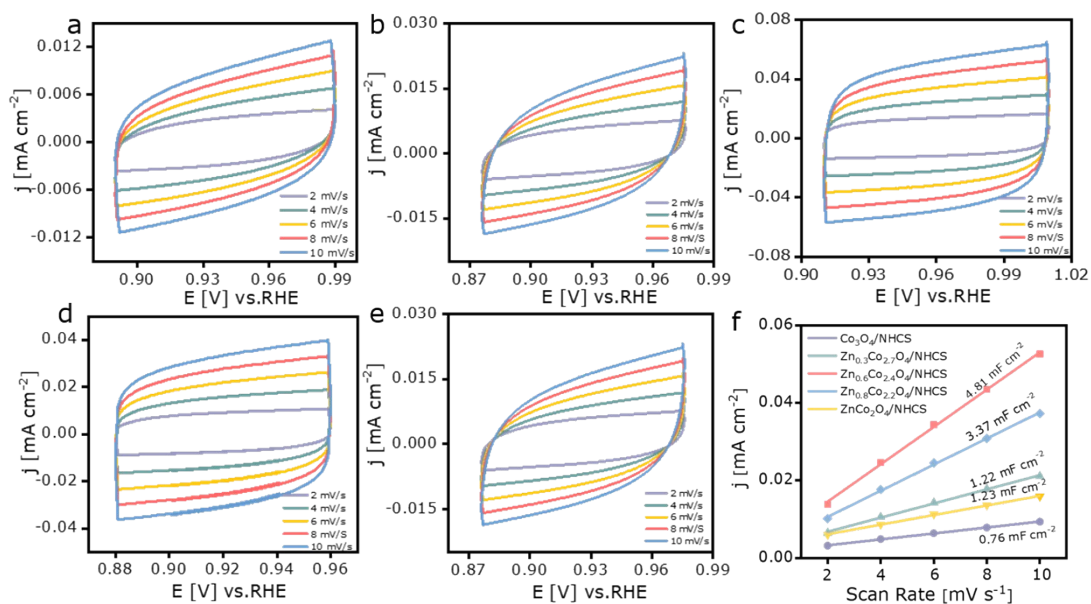


**Figure S8.** (a-f) CV curves of  $Zn_xCo_{3-x}O_4/NHCS$  at different scan rates and the calculated double layer capacitance of  $Zn_xCo_{3-x}O_4/NHCS$ .

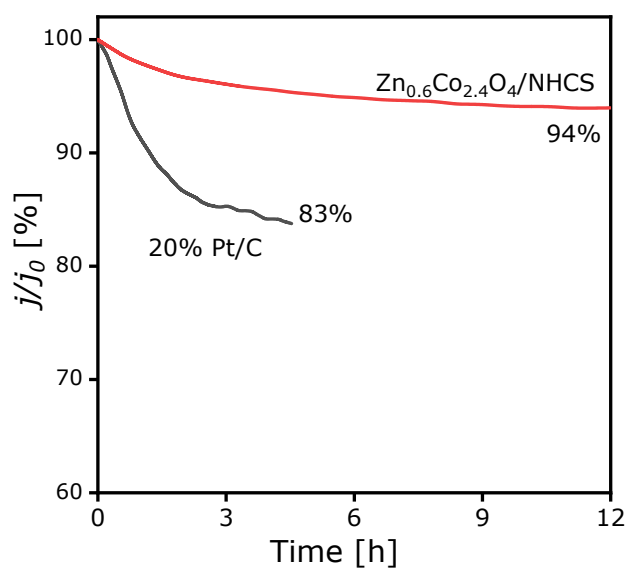


**Figure S9.** Chronoamperometric curves of  $Zn_{0.6}Co_{2.4}O_4/NHCS$  and Pt/C at ORR operating potential 0.4 V vs. RHE.

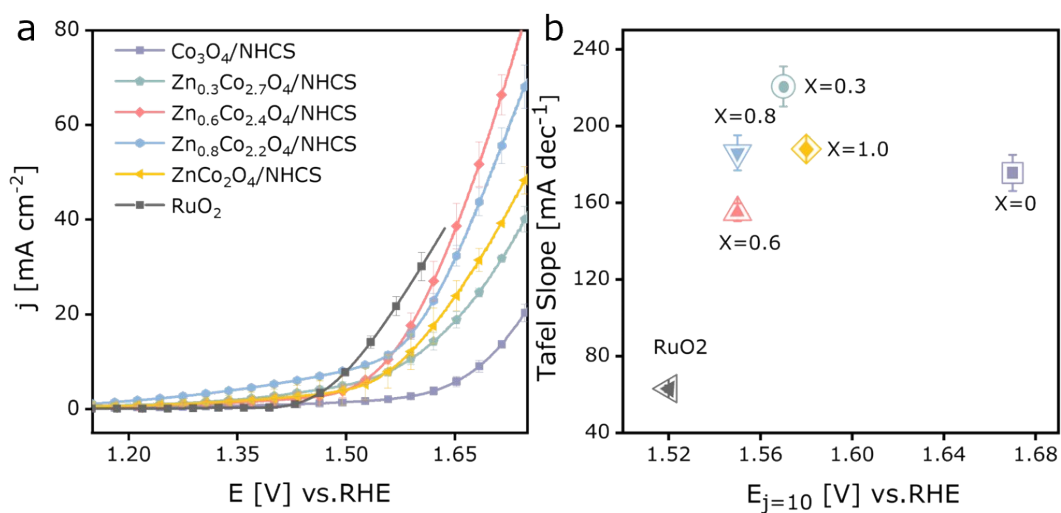


**Figure S10.** (a) OER polarization curves of  $Zn_xCo_{3-x}O_4/NHCS$  and  $RuO_2$  in 1 M KOH, (b) corresponding Tafel plots. Error bars represent the standard deviation from at least three independent measurements.

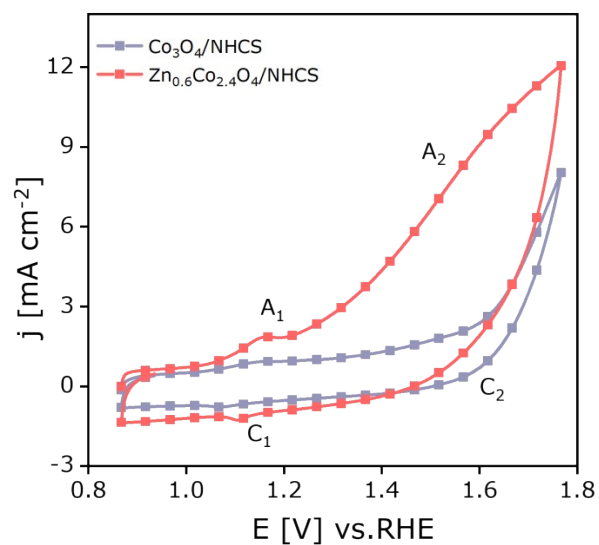


**Figure S11.** Cyclic voltammograms at the first cycle of  $Zn_xCo_{3-x}O_4/NHCS$  ( $x = 0, 0.6$ ) at 1 M KOH.

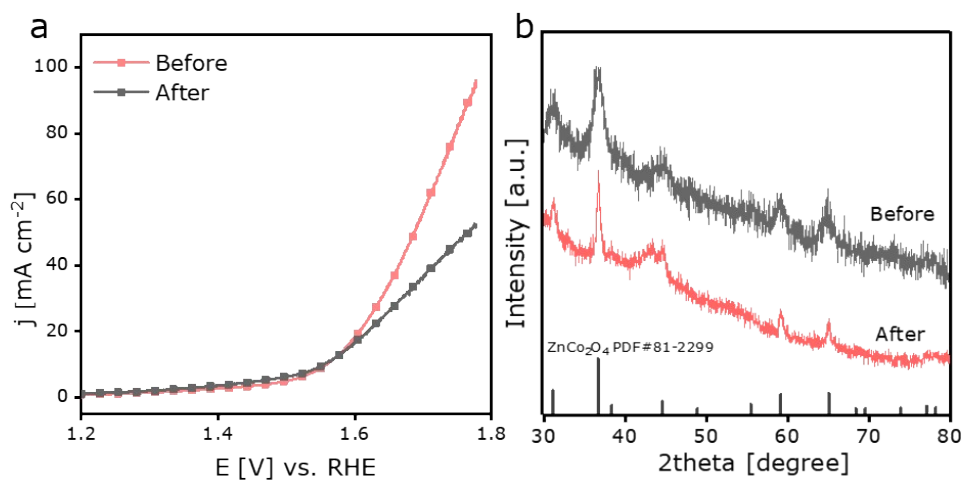


**Figure S12.** (a) Zn<sub>0.6</sub>Co<sub>2.4</sub>O<sub>4</sub>/NHCS OER LSV before and after 1500 voltametric cycles between 1.20 and 1.80 V vs. RHE, (b) XRD pattern of the sample before and after 1500 cycling.

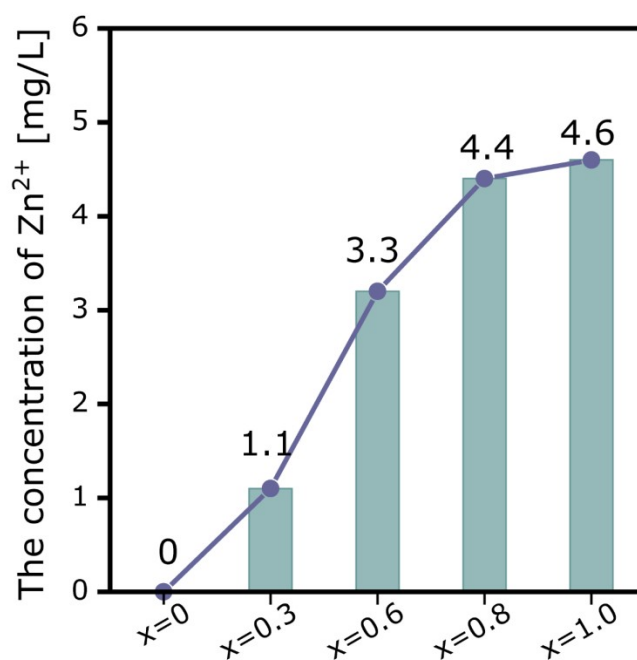


**Figure S13.** The amount of dissolved Zn<sup>2+</sup> in the sample after 1500 cycles.

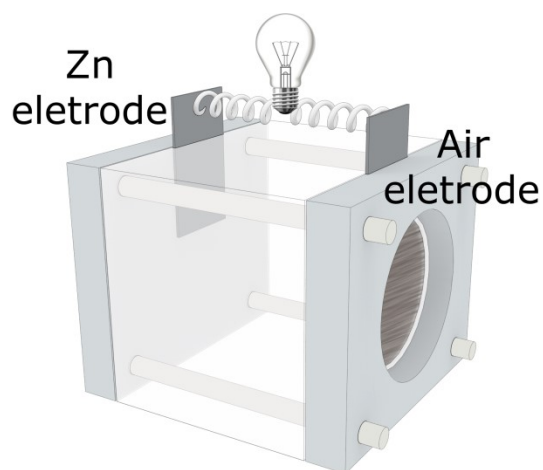


**Figure S14.** Scheme of  $\text{Zn}_{0.6}\text{Co}_{2.4}\text{O}_4/\text{NHCS}$  applied as cathode in Zn–air battery.

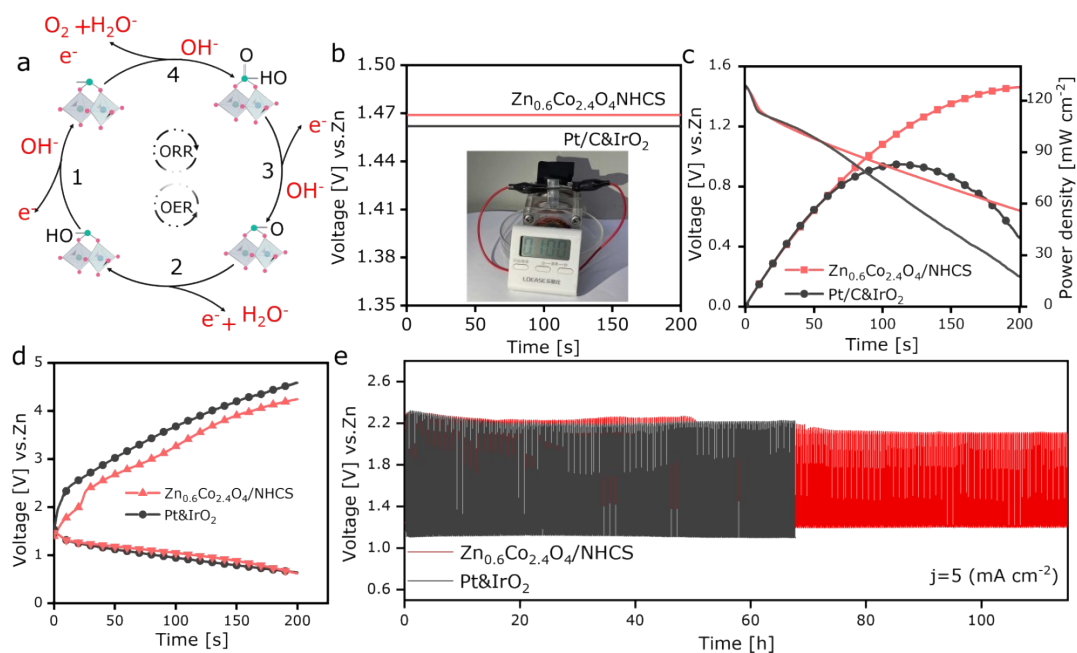


**Figure S15.** (a) Schematic diagram of ORR and OER, (b) the open-circuit voltage (inset: the practical application of equipped Zn–air battery with  $\text{Zn}_{0.6}\text{Co}_{2.4}\text{O}_4/\text{NHCS}$ ), (c) power density curves, (d) charge and discharge polarization curves of Zn–air batteries with catalysts, (e) long-term cycling performance at  $5 \text{ mA cm}^{-2}$  for 120 h.

## Supplementary Table

**Table S1.** Comparison of the electrocatalytic ORR activity of recent reported catalysts.

| Catalyst   | $E_{\text{onset}}$<br>(V) | $J_L$<br>(mA cm <sup>-2</sup> ) | Mass Loading<br>[mg cm <sup>-2</sup> ] | Tafel slope<br>[mV dec <sup>-1</sup> ] | Reference        |
|--|---------------------------|---------------------------------|--|--|------------------|
| <b>Zn<sub>0.6</sub>Co<sub>2.4</sub>O<sub>4</sub>/NHCS</b>                  | <b>0.87</b>               | <b>5.05</b>                     | <b>0.2</b>                             | <b>67</b>                              | <b>This work</b> |
| D-AC@2Mn-4Co   | 0.88                      | 4.72                            | 0.16                                   | 37.5                                   | 11               |
| Mn <sub>0.5</sub> Ni <sub>0.5</sub> Co <sub>2</sub> O <sub>4</sub><br>3DOM | 0.79                      | 5.67                            | 0.2                                    | 94                                     | 12               |
| Ni <sub>0.5</sub> Co <sub>2.5</sub> O <sub>4</sub>                         | 0.79                      | 5.11                            | 0.27                                   | 102.7                                  | 13               |
| NiCo <sub>2</sub> O <sub>4</sub>   | 0.89                      | 2.5                             | -                                      | 179                                    | 14               |
| MnCo <sub>2</sub> O <sub>4</sub> /C  | 0.85                      | 5.3                             | 0.127                                  |  | 15               |
| MnCo <sub>2</sub> O <sub>4</sub> /3D-G                                     | 0.98                      | 4.7                             | 0.25                                   | 70.2                                   | 16               |
| FeCoNiO <sub>x</sub> @IrPt   | 0.88                      | 4.7                             | 0.05                                   | 44                                     | 17               |
| MnCo <sub>2</sub> O <sub>4</sub> /NMCNA                                    | 0.90                      | 4.62                            | 0.1                                    | -                                      | 18               |
| 1D-Co <sub>3</sub> O <sub>4</sub>  | 0.82                      | 5.05                            | -                                      | -                                      | 19               |

**Table S2.** Comparison of the electrocatalytic OER activity of recent reported catalysts.

| Catalyst  | Overpotential at 10 mA cm <sup>-2</sup> | Tafel slope [mV dec <sup>-1</sup> ] | Mass Loading [mg cm <sup>-2</sup> ] | Solution                             | Reference        |
|---|---|-------------------------------------|-------------------------------------|--------------------------------------|------------------|
| <b>Zn<sub>0.6</sub>Co<sub>2.4</sub>O<sub>4</sub>/NHCS</b> | <b>310</b>                              | <b>156</b>                          | <b>0.2</b>                          | <b>1 M KOH</b>                       | <b>This work</b> |
| NiCo <sub>2</sub> O <sub>4</sub>                          | ~ 400                                   | 87                                  | 3                                   | 1 M KOH                              | 20               |
| Co <sub>3</sub> O <sub>4</sub> @C/CP                      | ~370                                    | 112                                 | —                                   | 0.5 M H <sub>2</sub> SO <sub>4</sub> | 21               |
| Co-CNT/PC   | ~300                                    | 73.8                                | 1                                   | 0.1 M KOH                            | 22               |
| Co <sub>3</sub> O <sub>4</sub> NS/ZTC                     | ~380                                    | 95                                  | 0.18                                | 1 M KOH                              | 23               |
| Mo-Co <sub>3</sub> O <sub>4</sub> /CNTs                   | ~270                                    | 63                                  | 0.25                                | 1 M KOH                              | 24               |
| NC-Co <sub>3</sub> O <sub>4</sub>                         | ~350                                    | —                                   | 0.25                                | 1 M KOH                              | 25               |
| Co@C-MWCNTs   | ~270                                    | 116                                 | 0.32                                | 1 M KOH                              | 26               |
| Co <sub>3</sub> O <sub>4</sub> /N-ACCNF                   | ~310                                    | 88                                  | 1.5                                 | 1 M KOH                              | 27               |
| 1D-Co <sub>3</sub> O <sub>4</sub>                         | ~320                                    | 70                                  | —                                   | 1 M KOH                              | 28               |

## Reference

1. C. Wei, R. R. Rao, J. Peng, B. Huang, I. E. L. Stephens, M. Risch, Z. J. Xu and Y. Shao-Horn, *Adv Mater*, 2019, **31**, 1806296.
2. C. Feng, F. Wang, Z. Liu, M. Nakabayashi, Y. Xiao, Q. Zeng, J. Fu, Q. Wu, C. Cui, Y. Han, N. Shibata, K. Domen, I. D. Sharp and Y. Li, *Nat. Commun.*, 2021, **12**, 5980
3. X. Liu, S. Xi, H. Kim, A. Kumar, J. Lee, J. Wang, N. Q. Tran, T. Yang, X. Shao, M. Liang, M. G. Kim and H. Lee, *Nat. Commun.*, 2021, **12**, 5676.
4. T. Wu, S. Sun, J. Song, S. Xi, Y. Du, B. Chen, W. A. Sasangka, H. Liao, C. L. Gan, G. G. Scherer, L. Zeng, H. Wang, H. Li, A. Grimaud and Z. J. Xu, *Nat. Catal.*, 2019, **2**, 763–772.
5. P. Zhai, Y. Zhang, Y. Wu, J. Gao, B. Zhang, S. Cao, Y. Zhang, Z. Li, L. Sun and J. Hou, *Nat. Commun.*, 2020, **11**, 5462.
6. X. Yan, J. Biemolt, K. Zhao, Y. Zhao, X. Cao, Y. Yang, X. Wu, G. Rothenberg and N. Yan, *Nat. Commun*, 2021, **12**, 4143.
7. J. Huang, H. Sheng, R. D. Ross, J. Han, X. Wang, B. Song and S. Jin, *Nat. Commun.*, 2021, **12**, 3036.
8. S. Xiao, D. Pan, R. Liang, W. Dai, Q. Zhang, G. Zhang, C. Su, H. Li and W. Chen, *Appl. Catal. B Environ.*, 2018, **236**, 304–313.
9. Gyutae Nam, M. C. Joohyuk Park, Pilgun Oh, Suhyeon Park, Min Gyu Kim, Noejung Park, Jaephil Cho, and and Jang-Soo Lee, *ACS Nano*, 2015, **9**, 6493–6501.
10. W. Lu, R. Jiang, X. Yin and L. Wang, *Nano Res.*, 2018, **12**, 159–163.
11. X. Yan, Y. Jia, J. Chen, Z. Zhu and X. Yao, *Adv. Mater.*, 2016, **28**, 8771–8778.
12. J. Béjar, L. Álvarez-Contreras, F. Espinosa-Magaña, J. Ledesma-García, N. Arjona and L. G. Arriaga, *Electrochim. Acta*, 2021, **391**, 138900.
13. J. Béjar, L. Álvarez-Contreras, J. Ledesma-García, N. Arjona and L. G. Arriaga, *J. Mater. Chem. A*, 2020, **8**, 8554–8565.
14. S. V. Devaguptapu, S. Hwang, S. Karakalos, S. Zhao, S. Gupta, D. Su, H. Xu and G. Wu, *ACS Appl. Mater.*, 2017, **9**, 44567–44578.
15. G. Fu, Z. Liu, J. Zhang, J. Wu, L. Xu, D. Sun, J. Zhang, Y. Tang and P. Chen, *Nano Res.*, 2016, **9**, 2110–2122.

16. T. Zhang, Z. Li, L. Wang, P. Sun, Z. Zhang and S. Wang, *ChemSusChem*, 2018, **11**, 2730–2736.
17. M. Wu, M. Cui, L. Wu, S. Hwang, C. Yang, Q. Xia, G. Zhong, H. Qiao, W. Gan, X. Wang, D. Kline, M. R. Zachariah, D. Su, T. Li and L. Hu, *Adv. Energy Mater.*, 2020, **10**, 200119.
18. D. Bin, Z. Guo, A. G. Tamirat, Y. Ma, Y. Wang and Y. Xia, *Nanoscale*, 2017, **9**, 11148–11157.
19. S. Dresp and P. Strasser, *ChemCatChem*, 2018, **10**, 4162–4171.
20. J. Béjar, L. Álvarez-Contreras, J. Ledesma-García, N. Arjona and L. G. Arriaga, *J. Electroanal. Chem.*, 2019, **847**, 113190.
21. X. Yang, H. Li, A.-Y. Lu, S. Min, Z. Idriss, M. N. Hedhili, K.-W. Huang, H. Idriss and L.-J. Li, *Nano Energy*, 2016, **25**, 42–50.
22. S. Dou, X. Li, L. Tao, J. Huo and S. Wang, *Chem. Commun*, 2016, **52**, 9727–9730.
23. R. K. Bera, H. Park and R. Ryoo, *J. Mater. Chem. A*, 2019, **7**, 9988–9996.
24. K. Lu, T. Gu, L. Zhang, Z. Wu, R. Wang and X. Li, *Chem. Eng. J.*, 2021, **408**, 127352.
25. C. Guan, A. Sumboja, H. Wu, W. Ren, X. Liu, H. Zhang, Z. Liu, C. Cheng, S. J. Pennycook and J. Wang, *Adv. Mater*, 2017, **29**, 1704117.
26. X. Li, Y. Fang, X. Lin, M. Tian, X. An, Y. Fu, R. Li, J. Jin and J. Ma, *J. Mater. Chem. A*, 2015, **3**, 17392–17402.
27. L. Qiu, X. Han, Q. Lu, J. Zhao, Y. Wang, Z. Chen, C. Zhong, W. Hu and Y. Deng, *Chem. Frontiers*, 2019, **6**, 3554–3561.
28. Q. Ren, Z. Feng, S. Mo, C. Huang, S. Li, W. Zhang, L. Chen, M. Fu, J. Wu and D. Ye, *Catal. Today*, 2019, **332**, 160–167.